Thermal vibrational amplitudes of constituent atoms and mechanical stability in $Zn_xCd_{1-x}Te$ and $Hg_{1-y}Cd_yTe$

D. Comedi* and R. Kalish
Physics Department and Solid State Institute, Technion–Israel Institute of Technology, 32000 Technion City, Haifa, Israel
(Received 25 June 1992; revised manuscript received 2 September 1992)

Root-mean-square (rms) displacements of the constituent atoms in the $Zn_xCd_{1-x}Te$ ($x=0,0.04,0.077,0.114,0.20,0.31$) and $Hg_{1-y}Cd_yTe$ ($y=0,0.24,0.4,0.7$) alloys are determined by ion channeling experiments combined with particle-induced x-ray emission and Rutherford backscattering. The experimental channeling angular scan data are interpreted by using a recently developed method, which uses a Monte Carlo simulation program of the channeling process, and includes a structural model for the ternary alloys based on extended x-ray-absorption fine-structure results on nearest-neighbor distances. Temperature-dependent measurements show that the experimentally deduced atomic displacements do not contain static contributions but they are rather due to the thermal vibrational amplitudes of the atoms. The room-temperature results are found to be in general agreement with the few thermal amplitude data reported in the literature obtained by other experimental methods. For both $Zn_xCd_{1-x}Te$ and $Hg_{1-y}Cd_yTe$ the rms displacements change nonmonotonically with composition. In some cases, the results are found to correlate with the experimentally determined bulk moduli and microhardness. The above correlations deduced from the present experiment for $Hg_{1-y}Cd_yTe$ and $Zn_xCd_{1-x}Te$ are found to be common to other tetrahedrally bonded semiconductors. Temperature-dependent results for $Zn_xCd_{1-x}Te$ crystals which show a strong reduction in thermal amplitudes as compared to CdTe at room temperature reveal deviations from the Debye behavior, not observed for the other materials studied. Possible explanations for the effects observed, as well as their implications to the phonon-dispersion relations of the ternary alloys studied, are discussed in detail.

I. INTRODUCTION

One of the basic issues regarding zinc-blende pseudobinary semiconductors $A_{1-x}B_xC$ is how their physical properties are related to those of the binary constituents AC and BC, and how these change with the molar concentration x of BC. Of special interest in this context are the II-VI based pseudobinary semiconductor alloys $Zn_xCd_{1-x}Te$ and $Hg_{1-y}Cd_yTe$, for which extensive investigations are being carried out, partially as a result of their increasing technological applications as infrared detectors, solar cells, and other devices.[1] In order to gain a basic understanding of the properties of pseudobinary semiconductor alloys in general, and of $Zn_xCd_{1-x}Te$ and $Hg_{1-y}Cd_yTe$ in particular, much effort has been devoted recently to calculating their electronic and structural properties,[2–4] and their thermodynamic properties[5,6] using first-principles[3,4] as well as empirical[2,5,6] theories. Theoretical predictions such as alloy structural disorder due to bond relaxation[3,7–9] have been confirmed by extended x-ray-absorption fine-structure (EXAFS) measurements of nearest-neighbor distances for $Zn_xCd_{1-x}Te$.[10] Nonrandom distributions of atoms in the mixed sublattice (i.e., clustering) are expected theoretically[5,8,9] and have been observed experimentally by nuclear magnetic resonance (NMR) measurements in both $Hg_{1-y}Cd_yTe$ (Ref. 11) and $Zn_xCd_{1-x}Te$,[12] and by Raman scattering measurements[13] in $Hg_{1-y}Cd_yTe$. More recently, x-ray diffraction studies have shown that coherent deviations from the zinc-blende structure may exist in $Zn_xCd_{1-x}Te$,[14], which are responsible for the unexpected ferroelectric properties detected at room temperature in these crystals.[15] Despite the importance that bonding and structural aspects have in determining the lattice dynamics and the mechanical stability of these materials, the implications of both recent theoretical and experimental findings on the atomic vibrations of constituent atoms in $Zn_xCd_{1-x}Te$ and $Hg_{1-y}Cd_yTe$ are still lacking. In fact, the experimental and theoretical knowledge on the lattice dynamics of these materials is rather limited. Phonon-dispersion relations have been measured by neutron diffraction only for the binary constituents CdTe, HgTe, and ZnTe.[16–19] Phenomenological models of lattice vibrations, such as the shell model or rigid ion model (RIM),[17,18] yield good overall fits to the experimental data for the zinc-blende constituents, at the expense of using a large number of free parameters in the fitting procedures. Optical Raman scattering and infrared absorption and reflection measurements have been used to determine the TO phonon frequencies at critical points of the Brillouin zone and their low-temperature composition dependence.[20–25] For both $Zn_xCd_{1-x}Te$ (Refs. 20–23) and $Hg_{1-y}Cd_yTe$ (Refs. 13, 24, and 25) a two-mode behavior has been found. In general, the random element isodisplacement model (REI) (Refs. 20 and 25) provides reasonable fits to the measured frequencies as a function of composition only when unphysical assumptions are made regarding the magnitude of interactions between

next-nearest neighbors. For $Zn_xCd_{1-x}Te$, the TO mode corresponding to CdTe shows an unusual dependence on composition which is presently not understood.[23] Although the atomic thermal vibrational amplitudes have been measured by diffraction methods for the binaries CdTe,[26] ZnTe,[27] and (to a lesser extent) HgTe,[28] little is known about the thermal amplitudes of atomic constituents in $Zn_xCd_{1-x}Te$ and $Hg_{1-y}Cd_yTe$ alloys. In diffraction measurements in polyatomic crystals the experimentally determined diffracted intensities are fitted by a convolution of a static structure factor with a temperature-dependent vibrational factor, the latter including contributions from *all* the vibrating atoms in the crystal. Therefore the problem of determining the individual atomic root-mean-square (rms) displacements from diffraction experiments requires the deconvolution of the temperature factor from the static structure factor. This procedure involves the *a priori* assumption of a model for the dynamic behavior of the different constituent atoms in the crystal. The direct measurement of the individual vibrational amplitudes of constituent atoms in $Zn_xCd_{1-x}Te$ and $Hg_{1-y}Cd_yTe$ and the study of their dependence on composition and temperature, as described here, is very desirable. It offers information about the potential well in which each particular atom vibrates, and through it about the local bonding properties and their changes with composition.[29]

In the present work we study the rms displacements of constituent atoms $Zn_xCd_{1-x}Te$ (x=0,0.04,0.077, 0.114,0.20,0.31) and $Hg_{1-y}Cd_yTe$ (y=0,0.24,0.4,0.7) using ion channeling combined with particle-induced x-ray emission (PIXE) and Rutherford backscattering (RBS). In the present channeling experiments,[30] the crystal under study is bombarded by a 200-keV proton beam and the yield of the backscattered particles (RBS) and characteristic x rays emitted by the different constituent atoms (PIXE) are measured as a function of tilt angle off the $[\bar{1}\,\bar{1}\,\bar{1}]$ crystallographic axis with respect to the beam. Under optimal channeling conditions, the projectiles are steered along the open channels of the crystal, never getting closer to the atomic rows than a minimum distance, which is of the order of 10^{-1} Å. Since the impact parameters required for L-shell ionization and for direct backscattering are of the order of 10^{-2} ad 10^{-4} Å, respectively, both RBS and PIXE spectra measured under channeling conditions show a strong reduction in yield and typical RBS and PIXE channeling angular scan curves (channeling dips) can readily be obtained. The velocities of the channeled particles are such that the time of interaction with a particular atom in the atomic row is very short as compared to the period of thermal vibrations of the atom. The particles thus interact with a "frozen" lattice, the atoms being displaced from their normal lattice sites with a certain statistical distribution. When the atomic rows contain different atomic species, as is the case for the ⟨111⟩ channels in the zinc-blende structure, the interaction probability between the channeled particles and the atomic species i will be proportional to u_1^i, where u_1^i is the corresponding one-dimensional rms displacement in the plane perpendicular to the channel. Different atoms having different u_1^i will therefore yield different measured channeling angular scan curves. Therefore, in contrast to diffraction methods where the diffracted intensities contain contributions from all the constituent atoms in the crystal, the present ion channeling-PIXE-RBS technique is an atom-sensitive probe[30] which allows for the determination of the rms displacements of Zn, Cd, Hg, and Te in $Zn_xCd_{1-x}Te$ and $Hg_{1-y}Cd_yTe$ individually.

The experimental channeling angular scan data are interpreted through a Monte Carlo simulation of the channeling process, which includes a structural model for the ternary alloys based on EXAFS results for nearest-neighbor distances. The structural model used in the simulation is described in Sec. III. Temperature-dependent measurements show that the atomic displacements deduced do not contain static contributions, i.e., they represent pure thermal vibrational amplitudes of the atoms. The results obtained at room temperature are found to correlate with previous data on mechanical properties of the studied alloys, such as the bulk moduli and microhardness. These correlations, and the implications of the present results to the phonon-dispersion relations of the ternary alloys studied, are discussed in Sec. IV.

II. EXPERIMENTAL PROCEDURE

A. Sample preparation

The $Zn_xCd_{1-x}Te$ samples (x=0,0.04,0.077,0.114, 0.2,0.31) were grown by the modified Bridgman method.[31] The Zn content for the x=0.114 and 0.077 samples was determined to within an accuracy of 3% by the double-crystal x-ray diffraction method, using the measured dependence of the lattice parameter on composition reported in the literature.[32] The composition of the other $Zn_xCd_{1-x}Te$ crystals was deduced from the relative intensities of the Cd, Zn, and Te $L_{\alpha\beta}$ peaks in the PIXE spectra measured at a random angle of beam incidence. The x values obtained this way were always very close to the nominal ones. The $Hg_{1-y}Cd_yTe$ samples (y=0,0.24,0.4,0.7) were grown by the traveling heater method.[33] All crystals were ⟨111⟩ oriented by x-ray diffraction, cut, mechanically polished by 5-, 0.3-, and 0.05-μm alumina powder, and finally chemically etched with 5% solution of Br_2 in methanol. The crystallographic polarity characteristic of the {111} faces of zinc-blende crystals, which is of importance in the present experiments,[30] was determined by the etching procedures outlined by Fewster *et al.*[34] and was confirmed in most cases by the ion channeling measurements.

B. Channeling measurements

For the channeling experiments, the ⟨111⟩-oriented samples were mounted on a 3-axis goniometer having an angular resolution of 0.01°. A proton beam accelerated to an energy of 200 keV was collimated to an angular definition better than 0.02°, and allowed to impinge on the crystal samples. The backscattered protons were detected with a surface barrier detector set at an angle of

165°, while characteristic x rays were detected with a Si (Li) detector at an angle of 135° with respect to the beam. Both RBS and PIXE spectra were recorded simultaneously for each crystal tilt angle, scanning through the $[\bar{1}\bar{1}\bar{1}]$ channel, typically at 0.1° or 0.2° increments. The angular scan curves for each element in the crystal were extracted from the PIXE spectra by integrating over the L lines of Zn, Cd, Te, and the M lines of Hg. Raw data of such angular scans are shown in Fig. 1 for Hg, Cd, and Te obtained for 200-keV protons incident on $[\bar{1}\bar{1}\bar{1}]$ $Hg_{0.76}Cd_{0.24}Te$.

The proton beam current density was kept lower than 1 nA/mm^2 in order to minimize sample heating. After a present charge density had been accumulated, the beam was moved to a fresh spot on the target in order to minimize damage production by the probing beam. The target holder could be cooled by a liquid-nitrogen Dewar, and the temperature could be continuously varied ($100 < T < 450$ K) by heating the cooling finger. The temperature was controlled within 2 K by a thermocouple placed on the sample holder close to the sample. The chamber was held at a pressure of 5×10^{-7} Torr. A cylindrical cryoshield at liquid-nitrogen temperature was placed surrounding the sample assembly in order to reduce impurity condensation on the sample surface during the low-temperature measurements.

C. Data interpretation

In the continuum model of channeling,[35] the channeled particles are assumed to interact with a momentarily "frozen" lattice, the atoms being displaced from their normal lattice sites with a spatial distribution P, which is generally assumed to be described by a Gaussian function with a standard (one-dimensional) deviation u_1, the thermal vibrational amplitude. The interaction probability χ between the flux of channeled particles F and the target atoms can be expressed by[35]

$$\chi(\psi) = \int F(\boldsymbol{\rho}, \psi) P(\boldsymbol{\rho}) d\boldsymbol{\rho} \ . \tag{1}$$

Here $\boldsymbol{\rho}$ is the position vector relative to the atomic row in the plane perpendicular to the channel and ψ is the angle of the incident beam with respect to the channel direction. The flux $F(\boldsymbol{\rho}, \psi)$ is determined mainly by the transverse continuum potential due to the atomic rows bordering the channels. When different atomic species are present in the rows, the fact that channeled trajectories have typical wavelengths of the order of a few hundred atomic spacings suggests that it is the average atomic charge which mainly determines the effective transverse potential and hence the flux F in such a case. The same argument applies when different interatomic spacings are present along the atomic rows,[36] as is the case for the $\langle 111 \rangle$ strings in the zinc-blende structure. However, it is the individual displacement distribution of each constituent atom $P(\boldsymbol{\rho})$ which will determine the degree of interaction between the channeled projectiles and the different atoms. Atomic species having different $P(\boldsymbol{\rho})$ (and different rms displacements) will therefore yield different measured channeling angular scan curves. This is the basis of the present experiment.

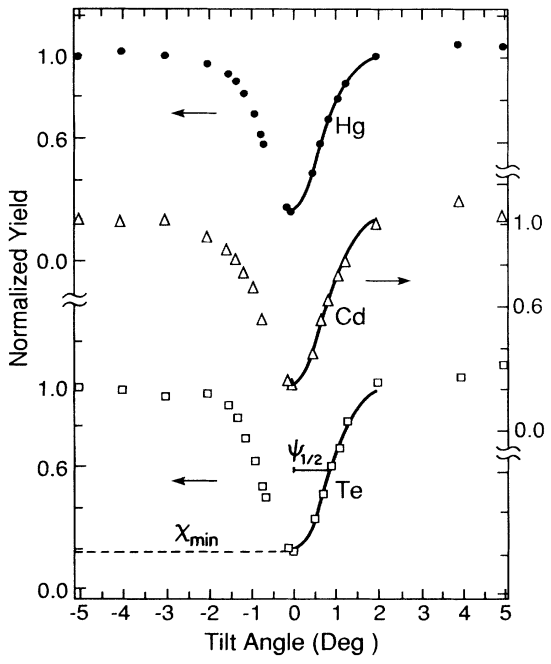

FIG. 1. PIXE angular scans through $[\bar{1}\bar{1}\bar{1}]$ of Hg $M_{\alpha\beta}$ (●), Cd $L_{\alpha\beta}$ (△), and Te $L_{\alpha\beta}$ (□) induced by 200-keV protons in $Hg_{0.76}Cd_{0.24}Te$ at room temperature. The solid lines are results from Monte Carlo computer simulations (see text). The definitions of the channeling half-width $\psi_{1/2}$ and minimum yield χ_{min} are shown on the PIXE angular scan for Te.

The most straightforward way of obtaining channeling data is by measuring the backscattering yield of the channeled particles (Rutherford backscattering). Unfortunately, the limited elemental resolution of RBS does not permit a clear discrimination between particles backscattered from different constituent atoms in the materials studied in the present work, which contain atoms having rather similar masses (i.e., Cd and Te in CdTe, $Zn_xCd_{1-x}Te$, and $Hg_{1-y}Cd_yTe$), and light atoms distributed in a heavier matrix (i.e., Zn in CdTe). These elements can be discriminated by particle-induced x-ray emission.[30] The L shells of Zn, Cd, and Te and Hg M shells are easily excited by sub-MeV protons and the characteristic x rays emitted can be readily resolved. However, a known disadvantage of PIXE is its poor depth resolution. As the projectiles penetrate into the solid they gradually lose their energy, the probability for target atom inner shell excitation being reduced with depth. Furthermore, the x-ray photons emitted are partially self-absorbed in the crystal on their way out to the detector. As a result, measured PIXE channeling angular dips for different constituent atoms contain contributions from broad depth bins in the crystal. Since the characteristics of the channeled beam are also depth dependent, the different depths over which characteristic x rays emitted by different atoms originate must be considered. In the present work, the experimental angular scan data are interpreted by using two methods which overcome the above difficulties. These have been discussed in detail elsewhere,[30] and are therefore only briefly described below.

1. Method A

In this method, the half-widths $\psi_{1/2}^{\mathrm{PIXE},i}$ and minimum yields $\chi_{\min}^{\mathrm{PIXE},i}$ are extracted from the experimental PIXE channeling angular scans (see Fig. 1). The RBS channeling angular scan data, which are measured simultaneously with the PIXE data, are used to calculate depth correction factors for $\psi_{1/2}^{\mathrm{PIXE},i}$ and $\chi_{\min}^{\mathrm{PIXE},i}$. These calculations, which take advantage of the depth information contained in RBS spectra and make use of the published data on inner shell ionization cross sections[37] and the x-ray photon absorption probabilities,[38] have been described in detail elsewhere.[30] The individual rms atomic displacements u_1^i for each constituent atom i are determined from the corresponding depth corrected PIXE half-widths using the equations[30]

$$\psi_{1/2}^{\mathrm{PIXE},i}(0)=0.8\left\{\frac{Z_1\bar{Z}_2e^2}{Ed}\ln\left[\frac{3\bar{a}^2}{1.44(u_1^i)^2}+1\right]\right\}^{1/2} \tag{2}$$

while the corresponding depth corrected experimental PIXE minimum yields are checked to satisfy the equations

$$\chi_{\min}^{\mathrm{PIXE},i}(0)=6Nd\pi(u_1^i)^2\times\left[1+\left[\frac{\psi_{1/2}^{\mathrm{PIXE},i}(0)d}{2.2u_1^i}\right]^2\right]^{1/2}. \tag{3}$$

In Eqs. (2) and (3), the index 0 states that the PIXE channeling parameters have been corrected for the corresponding depth effects.[30] Z_1 is the atomic number of the projectile while $\bar{Z}_2$ and d are the weighted average of the atomic numbers of the crystal constituent atoms and the interatomic spacing along the rows, E is the beam energy, N is the atomic concentration, and $\bar{a}$ is the weighted average of the atomic Thomas-Fermi screening lengths.[36]

2. Method B

In this method, a simulation program of the channeling process is used.[39,30] The ion-atom interactions are described by Molière potentials. The particle trajectories and the nuclear energy loss are calculated within the binary collision model using the impulse approximation. The equilibrium position of different atoms in the crystal are selected taking the zinc-blende lattice structure as a basis. The crystal atoms are assumed to be displaced isotropically from their lattice sites, with a Gaussian displacement distribution having a one-dimensional standard deviation u_1^i, where i denotes the atom type. The quantity calculated by the program at any depth z is the nuclear encounter probability (NEP) (Refs. 39 and 30) between the channeled particles and the crystal atom i, which is given by[30]

$$P_i=\frac{\cos\psi}{2\pi[(u_1^i)^2+(r_i)^2]NdN_c}\times\sum_{j=1}^{N_c}\exp\left[-\frac{x_j^2+y_j^2}{2[(u_1^i)^2+(r_i)^2]}\right], \tag{4}$$

where ψ is the angle of incidence of the particle with respect to the channel direction, r_i is the mean impact parameter for the inner shell ionization of element i, x_j and y_j are the particle coordinates in the plane perpendicular to the channel, and N_c is the total number of calculated collisions. For the cases considered in this work $(r_i)^2\ll(u_1^i)^2$. The PIXE channeling angular dips for the element i are calculated using the expression[30]

$$P_i^{\mathrm{PIXE}}=\int P_i(z,\psi)\sigma_i[E(z,\psi)]\exp\left[-\frac{\mu_i z}{\cos\theta_x}\right]dz, \tag{5}$$

where P_i is the generalized NEP for element i as a function of depth [Eq. (4)], μ_i is the absorption coefficient of the x-ray photons emitted by the atom i,[38] θ_x is the angle between the x-ray detector and the sample normal, σ_i is the ionization cross section[37] of the inner shell considered, and E is the proton energy computed at the depth z. The individual rms atomic displacements u_1^i are deduced by directly fitting the simulated results [Eq. (5)] to the corresponding experimental PIXE angular scan curves.

III. STRUCTURAL MODEL FOR THE ALLOY $A_{1-x}B_xC$

The structure of pseudobinary alloys $A_{1-x}B_xC$ has been the subject of many theoretical and experimental studies. Early x-ray diffraction measurements[32] indicated a zinc-blende structure, with the lattice parameter changing almost linearly with composition between the binary constituents, in agreement with Vegard's law[40] and the virtual crystal approximation (VCA).[41] More recent EXAFS measurements in $In_xGa_{1-x}As$ (Ref. 42) and in similar alloys, including $Zn_xCd_{1-x}Te$,[10,43] have shown that local deviations from the zinc-blende structure exist. The main experimental evidences from EXAFS are[42,10] (1) the nearest-neighbor distances (bond lengths) in the alloy $A_{1-x}B_xC$ exhibit a bimodal distribution, one mode corresponding to the AC bond length and the other to BC, and (2) the next-nearest-neighbor distances for the mixed sublattice (A,B) approach the VCA limit, while the next-nearest-neighbor distances for the unmixed (C) sublattice shows a bimodal distribution.

Evidence (2) would mean that the structure of a mixed $A_{1-x}B_xC$ crystal is composed of a nearly perfect fcc (A,B) sublattice, with a strongly distorted (C) sublattice. For the purpose of the interpretation of the present channeling results, a simple structural model which is compatible with the EXAFS results above is adopted for the description of the crystals under study in the channeling simulation program. The model is similar (but not equivalent) to that proposed by Balzarotti.[5]

The $A_{1-x}B_xC$ lattice is simulated by taking the zinc-blende structure as a basis; a random distribution of a fraction x of atoms B on sites of the A sublattice is assumed. The mixed (A,B) sublattice is assumed to retain its fcc characteristic structure, while the unmixed sublattice (atoms C) is allowed to relax in such a way as to reproduce the experimentally observed AC and BC average bond lengths over the entire composition range. The

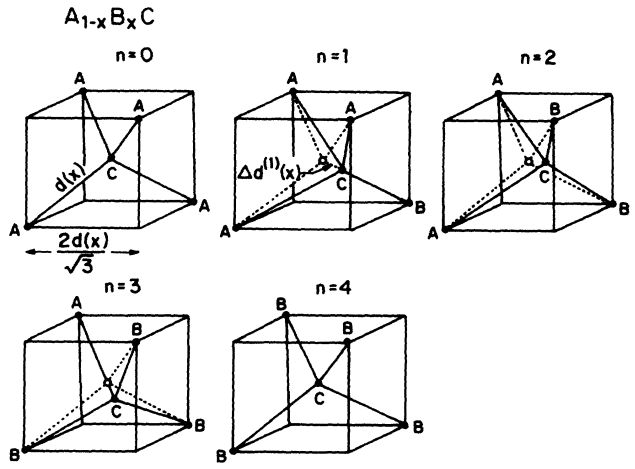

FIG. 2. Schematic description of the structural model for $A_{1-x}B_xC$ alloys used by the channeling simulation program (see text).

model is illustrated in Fig. 2, where the BC bond has been assumed to be shorter than the AC bond. There are five different possible configurations of nearest neighbors around the C atom, denoted by $n=0,1,2,3,4$ in the figure. In the ideal zinc-blende structure (i.e., in the VCA) atoms C would occupy the site at the center of each cubic cell. In the real alloy, however, the possible existence of two different kinds of atoms in the corners of the cells with different associated bond lengths, AC and BC, leads to static displacements of atoms C from the center of the cube. In the present model, the cubic unit cells defined by atoms A and B as depicted in Fig. 2 are assumed to have a side length $2d(x)/\sqrt{3}$, where $d(x)$ is the average bond length of the alloy as deduced from Vegard's law. This assumption is consistent with evidence (2) from EXAFS measurements. For the symmetric cases $n=0$ and 4 atom C remains undisplaced. The displacement of C along the BC bond for $n=1$ (see Fig. 2), $\Delta d^{(1)}$, is assumed to be given by

$$\Delta d^{(1)}(x)=\epsilon d(x) , \tag{6}$$

where ϵ is a free parameter of the model which is assumed to be constant with composition. The resultant displacements of atom C (magnitudes and directions) for $n=2,3$ are calculated by symmetry considerations, using Eq. (6) for the displacement component along the BC bonds. In the channeling simulations, for every C atom along the atomic row, its four nearest neighbors (i.e., A or B) are identified according to the relative composition x, and the corresponding displacement is calculated. The new atomic coordinates including both the static and the isotropic thermal displacements are then used for the calculation of the projectile scattering parameters. Note that while there are only three possible nonzero displacement magnitudes, there are 14 different displacement directions which are all included in the simulation calculations. The different Te sites allowed according to the present model for $\epsilon=0.045$ in $Zn_{0.1}Cd_{0.9}Te$ are depicted in Fig. 3. It can be seen that the displacement magnitudes are of the order of 0.12 Å in this case. It should be pointed out, however, that only those displacements having nonzero projection on the plane perpendicular to the channel direction (the x-y plane in Fig. 3) will have significant influence on the calculated scattering of the channeled particles.

The resulting distribution of bond lengths is also calculated by the program for comparison with the corresponding EXAFS data to enable the determination of the parameter ϵ. There are four different Cd—Te and Zn—Te bond lengths corresponding to the different configurations $n=0$ and 4,1,2,3, each occurring statistically according to the Bernoulli distribution. Figure 4 shows the average CdTe and ZnTe bond lengths in $Zn_xCd_{1-x}Te$ (solid lines) as calculated by the simulation program for $\epsilon=0.045$ and the corresponding experimental values as measured by EXAFS.[10] It can be seen that satisfactory agreement between theory and experiment is obtained.

An important disadvantage of the model is that it neglects any relaxation of the mixed (A,B) sublattice

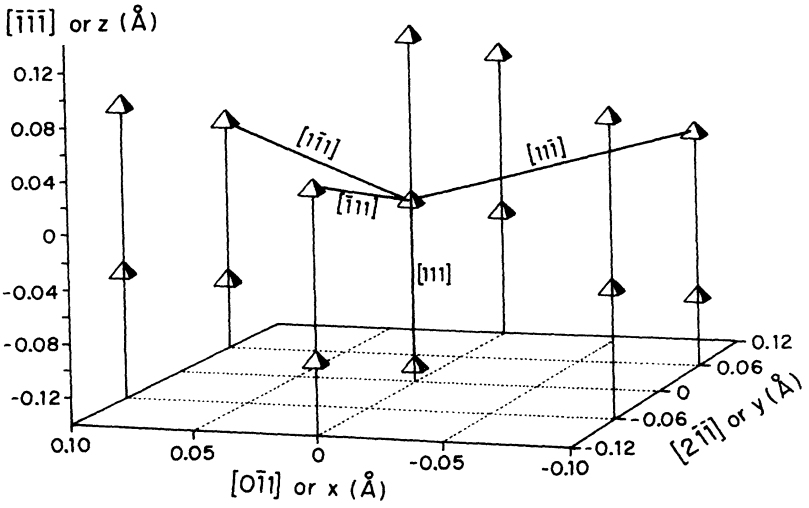

FIG. 3. Possible Te sites according to the present structural model in $Zn_{0.1}Cd_{0.9}Te$ for $\epsilon=0.045$. The $[\bar{1}\bar{1}\bar{1}]$ channeling direction is the positive direction parallel to the z axis.

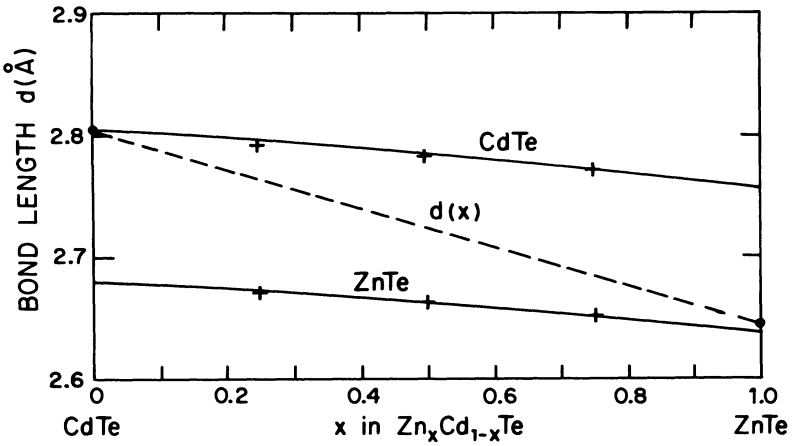

FIG. 4. Bond lengths as calculated by the simulation program (solid lines) for CdTe and ZnTe in $Zn_xCd_{1-x}Te$ as a function of x for $\epsilon=0.045$. The + symbols are the experimental values as determined by EXAFS measurements (taken from Ref. 10). Dashed line: average bond length calculated according to the VCA. ●: values deduced from the experimental lattice parameters (Ref. 32).

which according to calculations is likely to exist.[44] Although this neglect is partially justified by the consistency with EXAFS result (2) above, it may lead to some overestimation of the static displacement distribution of C atoms. The main quantity calculated by the simulation program to be directly compared to the experimental channeling results is the nuclear encounter probability (Sec. II C, method B) between the channeled particles and a specific atomic species in the lattice [Eq. (4)]. Figures 5 and 6 show the influence of the static displacements on the NEP as a function of depth (or number of atomic layers traversed) as calculated by the program for Cd and Te in $Zn_{0.3}Cd_{0.7}Te$. For this particular composition the value obtained for $\Delta d^{(1)}$ is 0.11 Å. The channeling calculations were done for two different cases: $u_1=0.06$ Å, for which $\Delta d^{(1)}>u_1$ (Fig. 5) and $u_1=0.14$ Å, for which $\Delta d^{(1)}<u_1$ (Fig. 6). In both cases the u_1 values have been assumed to be the same for Zn, Cd, and Te, and they roughly correspond to crystal temperatures of 100 and 293 K, respectively. It can be seen that when the vibrational amplitudes are smaller than the static displacements the NEP's for both Cd and Te are significantly increased when the static displacements of Te are included

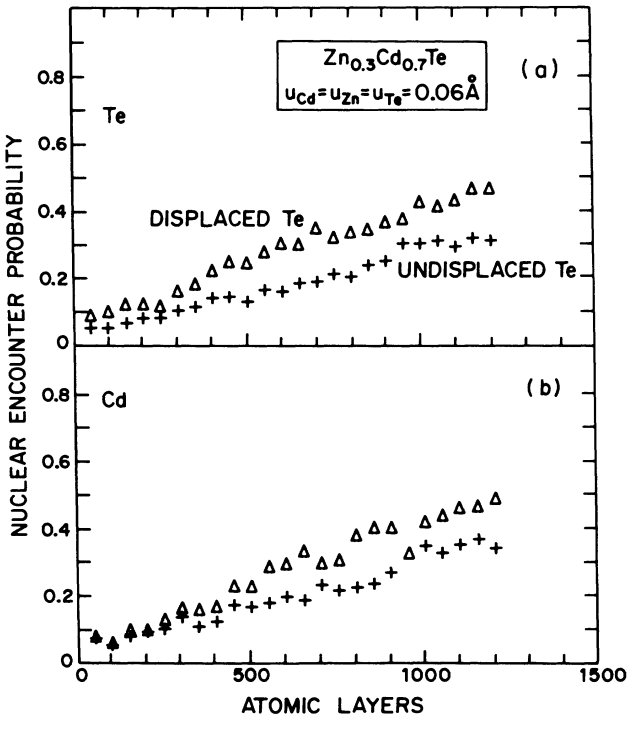

FIG. 5. Nuclear encounter probability (NEP) as a function of number of layers traversed by the channeled ion calculated for 200-keV protons incident at an angle of 0.8° with respect to the [111] axis of $Zn_{0.3}Cd_{0.7}Te$, assuming $u_1=0.06$ Å. (a) NEP for Te. (b) NEP for Cd. +, ideal zinc-blende structure; (△), with Te atoms displaced according to the present structural model.

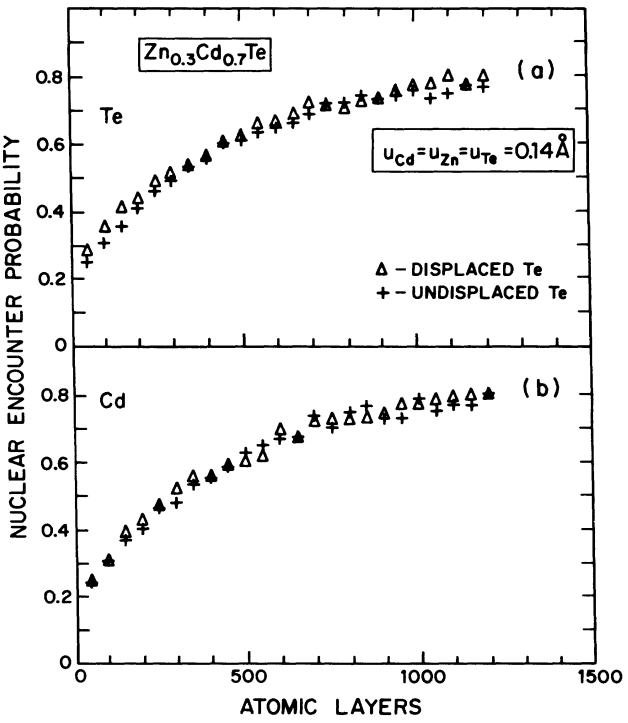

FIG. 6. Same as Fig. 5, but assuming $u_1=0.14$ Å.

(Fig. 5). However, for depths shallower than 250 atomic layers ($\approx$1400 Å) the calculated NEP for the Cd atoms is not influenced by the inclusion of static displacements. For the case where the vibrational amplitudes are larger than the static displacements (Fig. 6) the NEP's for Cd and Te remain almost unchanged upon inclusion of the static displacements, with only a small increase in the NEP of Te being observed at the shallow depth region. The above behavior can be qualitatively understood as follows: As the particles enter the lattice, the close encounter probability with Te atoms is increased relative to the zinc-blende case due to the static displacements of Te atoms [shallow depth region in Figs. 5(a) and 6(a)]. However, an indirect effect caused by the static displacements of Te is to gradually increase the scattering angle distribution of the channeled particles to higher angles. As a result, the calculated NEP's for both Cd and Te atoms at greater depths are higher than those calculated for the zinc-blende structure [Fig. 5(b)]. For the case in which $\Delta d^{(1)} < u_1$ (Fig. 6) the channeled trajectories and the NEP's are mainly determined by thermal vibrations of all the atoms, and therefore the influence of the inclusion of the Te atoms' static displacements is small.

IV. RESULTS AND DISCUSSION

A. Atomic displacements at room temperature

Figures 7(a) and 7(b) show the rms atomic displacements (u_1) as deduced from the channeling results for Cd and Te in $Zn_xCd_{1-x}Te$ ($0 \le x \le 0.31$) and for Hg, Cd, and Te in $Hg_{1-y}Cd_yTe$ ($0 \le y \le 1$). Note that in order to provide a common basis for a comparison between the results obtained for both pseudobinary systems, the u_1 results for $Hg_{1-y}Cd_yTe$ were plotted as a function of x (i.e., $x = 1-y$). The displacements obtained for Zn in the $Zn_xCd_{1-x}Te$ system are not shown in Fig. 7(a) for clarity; they follow the general trend with composition as depicted in Fig. 7(a), and are listed in Table I for completeness. Also shown in Fig. 7(a) are similar results from Mössbauer and diffraction experiments available from the literature for $Zn_xCd_{1-x}Te$ (Refs. 45 and 46) and for pure ZnTe.[27] It should be noted, however, that in contrast to the present channeling measurements from which the individual rms displacements of Zn, Cd, and Te are deduced, Mössbauer measurements give information on the vibrations of Te only (specifically the ^{125}Te isotope) and the diffraction study (Ref. 46) gives an average rms displacement over the individual displacements of the constituent atoms at each composition. As can be seen in Fig. 7(a), for the compositions where both channeling and Mössbauer data exist ($x = 0$ and $0.31-0.35$) the agreement between the rms displacements of Te atoms as determined by the two methods is good. Furthermore, there is a qualitative agreement between the channeling and the diffraction data. Both methods show a significant overall reduction in rms displacements for $x = 0.114$ relative to pure CdTe ($x = 0$), followed by an increase when going from $x = 0.114$ to $x \gtrsim 0.3$. It should be noted that while the presence of static displacements of Te atoms due to bond relaxation was taken into account in the analysis of the channeling results (see Sec. III), the x-ray diffraction data have not been corrected for such displacements. This is one possible reason for the tendency of the diffraction u_1 data points to be higher than the corresponding channeling results for the alloys. The atomic displacements as obtained by the ion channeling technique for Cd and Te in CdTe and for Hg and Te in HgTe are found, on the other hand, to be in close agreement[30] with similar data obtained by x-ray diffraction methods available from the literature.[26,28] It must be pointed out, however, that results from the diffraction method and ion channeling are not expected to be exactly the same. While the latter is essentially sensitive to the vibrations of the nuclei, diffraction measurements are also sensitive to the displacements of the core electrons. Furthermore, in compound crystals, different constituent atoms contribute collectively to the measured diffracted

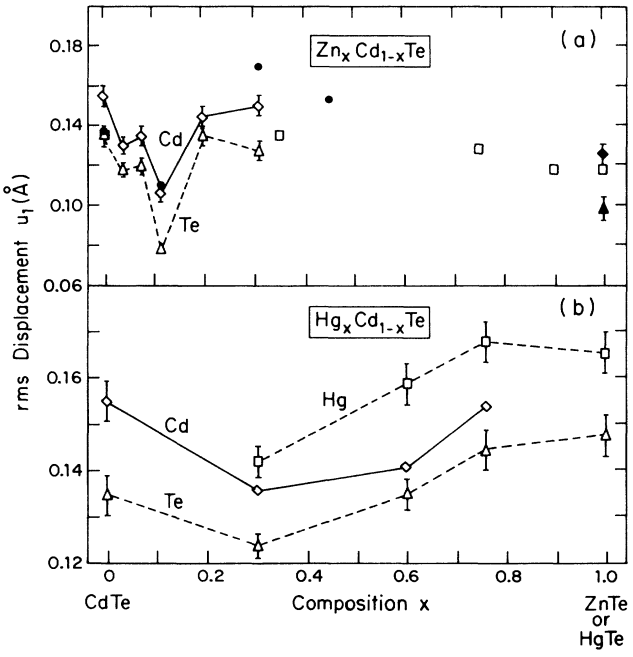

FIG. 7. rms displacements as deduced from the present channeling measurements for Cd, (◇), Te (△), and Hg (□) as a function of composition x in (a) $Zn_xCd_{1-x}Te$ and (b) $Hg_xCd_{1-x}Te$ at room temperature. Also shown in (a) are similar results obtained by diffraction methods (●) (Ref. 46), and by Mössbauer measurements for Te (□) (Ref. 45). The Mössbauer data have been extrapolated to room temperature. ♦, Zn in ZnTe; ▲, Te in ZnTe (Ref. 27).

TABLE I. Root-mean-square displacements as deduced from the present room-temperature channeling measurements for Zn in $Zn_xCd_{1-x}Te$ of various compositions.

x in $Zn_xCd_{1-x}Te$	u_1(Zn) (Å) ±0.005
0.04	0.125
0.077	0.129
0.114	0.095
0.20	0.140
0.31	0.148

intensities in diffraction experiments. In the present ion channeling method, in contrast, the projection of the rms displacement of each constituent atom in the plane perpendicular to the $[\bar{1}\,\bar{1}\,\bar{1}]$ channels is deduced directly from the angular dependence of its characteristic x rays, which are emitted individually and are clearly resolved in the measurements.[30]

One interesting observation that can be noted in Fig. 7 is that u_1 changes nonmonotonically with composition. For $Zn_xCd_{1-x}Te$ this is in contrast to the trend expected from recent RIM calculations[47] where the thermal amplitudes obtained for a "Zn-Cd pseudoatom" and for Te change monotonically between those of CdTe and ZnTe. In both pseudobinary systems a minimum in the rms displacements is found to be present within the studied composition ranges; for $Zn_xCd_{1-x}Te$ it is at $x \approx 0.1$ and for $Hg_{1-y}Cd_yTe$ at $y \approx 0.7$ ($x \approx 0.3$). However, the overall changes in u_1 obtained for the $Zn_xCd_{1-x}Te$ system are much more drastic than in $Hg_{1-y}Cd_yTe$. For both materials the anion (Te) atomic displacements are always lower than the cation atom displacements. This is in agreement with the general trend found in diffraction studies of thermal amplitudes in various III-V and II-VI binary compounds.[26,28,48] In $Hg_{1-y}Cd_yTe$ the displacements found for Hg are the highest for every composition, while for $Zn_xCd_{1-x}Te$ the displacements of Cd are the largest. This behavior suggests that the cation atom which vibrates with a larger rms displacement in its binary compound (i.e., Hg in HgTe as compared to Cd in CdTe and Cd in CdTe as compared to Zn in ZnTe, see Fig. 7), will also have the largest thermal amplitude in the corresponding alloy, regardless of the relation between their masses. The insensitivity of the thermal amplitudes to the mass of the vibrating atoms can be expected theoretically within the Debye model at temperatures above the Debye temperature.[49]

B. Correlation with mechanical properties

The general agreement obtained between the present experimental atomic displacements and the vibrational amplitudes inferred from diffraction studies, and the fact that the presence of static displacements due to bond relaxation has been taken into account in the analysis of the experimental data, suggest that the u_1 results displayed in Fig. 7 may be interpreted as being mainly vibrational in character. As will be shown below, the above interpretation is confirmed by temperature-dependent results. It is therefore justified to compare the present atomic displacements (u_1) with the available experimental data on

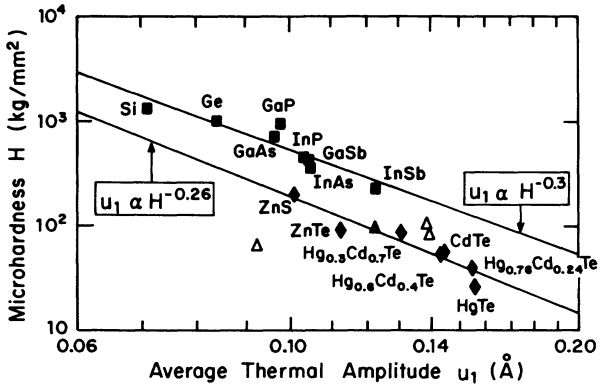

FIG. 8. Vicker microhardness (Refs. 51, 52, 56, and 58) vs the average thermal amplitudes for various IV, III-V, and II-VI semiconductors. The u_1 data for the II-VI semiconductors [except ZnTe (Ref. 27) and ZnS (Ref. 54)] are those determined in the present work. △, data for the $Zn_xCd_{1-x}Te$ alloys. ▲, data for $Zn_{0.04}Cd_{0.96}Te$.

mechanical properties of the materials under study, such as microhardness (H) and bulk modulus (B). For that purpose, a measured increase in u_1 is interpreted as being produced by a general weakening of the lattice (i.e., a decrease of the interatomic force constants and therefore a decrease in H and B). Similarly, a measured decrease in u_1 is attributed to a strengthening of the lattice.

The overall dependence of u_1 on composition in $Hg_{1-y}Cd_yTe$ was previously found by us[50] to be in qualitative agreement with trends in the microhardness observed in this system.[51] The measured microhardness for $Hg_{1-y}Cd_yTe$ as a function of composition presents a significant upwards bowing with respect to the weighted average of the microhardness values of HgTe and CdTe.[51] The microhardness maximum found at about $y=0.7$ is in agreement with the minimum in u_1 around the same composition found in the present work [see Fig. 7(b)]. Figure 8 shows Vicker microhardness experimental data for various IV, III-V, and II-VI (Refs. 52 and 53) semiconductors, including the data for $Hg_{1-y}Cd_yTe$, plotted against the corresponding vibrational amplitudes reported in the literature.[26–28,48] The u_1 data for the IV and III-V semiconductors were taken from the systematic diffraction measurements carried out by Nielsen *et al.*[48] It can be seen in Fig. 8 that a clear correlation exists between the measured Vicker microhardness and thermal amplitudes. The relationships

$$u_1 \propto H^{-\alpha} \begin{cases} \alpha = 0.30 & \text{for IV and III-V semiconductors} \quad (7a) \\ \alpha = 0.26 & \text{for II-VI semiconductors (except } Zn_xCd_{1-x}Te \text{ alloys, see below)} \quad (7b) \end{cases}$$

can be deduced from the figure. Furthermore, it can be noted that a gap exists between the line connecting the data for the IV and III-V semiconductors, and the corresponding line for the II-VI materials. The fact that all data for the II-VI semiconductors exhibit lower microhardness values than the corresponding group III-V and IV semiconductors may be associated with the lower structural stability which characterizes the II-VI compounds at high pressures[55] due to their higher bond ionicities. A similar gap between experimental values of the

microhardness of various III-V and II-VI semiconductors may be observed when plotting the data against the corresponding measured bulk moduli (see Fig. 11 below). Microhardness measurements as a function of composition for $Zn_xCd_{1-x}Te$ have been reported.[56] These show a significantly larger upwards bowing as compared to $Hg_{1-y}Cd_yTe$, having a maximum around $x=0.75$. The above behavior is in qualitative agreement with the results deduced from the present channeling measurements. Both show that the lattice is stiffer for the alloy than for pure CdTe and ZnTe, and that the detected hardening effects in $Zn_xCd_{1-x}Te$ are larger than those found in $Hg_{1-y}Cd_yTe$. However, the microhardness curve for $Zn_xCd_{1-x}Te$ increases monotonically from $x\approx 0.1$ towards the maximum at $x\approx 0.75$, in contrast to the present u_1 results which show a minimum at $x\approx 0.1$ [see Fig. 7(a)]. The microhardness results for $Zn_xCd_{1-x}Te$ (Ref. 56) are plotted against the presently deduced thermal amplitudes in Fig. 8 (open triangles); the clear deviation of the data points from the general behavior is noted. The above discrepancy may be related to the fact that $Zn_xCd_{1-x}Te$ alloys, in contrast to $Hg_{1-y}Cd_yTe$, are structurally distorted due to the presence of two very different (CdTe and ZnTe) bond lengths in this material.[10] As has been argued before,[56,57] the strain field produced by alloy disorder strongly influences the dislocation motion, thus affecting the measured microhardness. In fact, this argument has been frequently used to explain the "solid solution hardening" effect in various pseudobinary semiconducting systems.[56,57] The thermal vibrational amplitudes, in contrast, are expected to be determined mainly by the bonding properties of the crystal and not by dislocation kinetics. The fact that the data point corresponding to $Zn_{0.04}Cd_{0.96}Te$ (which among the studied $Zn_xCd_{1-x}Te$ alloys is the one having the lowest Zn content) agrees well with the correlation line (closed triangle in Fig. 8) may support the above speculation.

The general relationship found between the microhardness and the thermal amplitudes suggests that both quantities are basically determined by common factors. Correlations between the measured microhardness for the III-V binary compound semiconductors with bond length and ionicity in these materials have been previously noted.[58] Sher, Chen, and Spicer[53] used Harrison's tight-binding formulation of tetrahedral semiconductors to calculate the hardness of various group-IV semiconductors and III-V and II-VI binary compounds obtaining good qualitative agreement with the experimental trends.[53] The simple correlation found in the present work between the microhardness and the thermal amplitudes for some tetrahedral semiconductors, including $Hg_{1-y}Cd_yTe$, indicates that the microhardness, which is a macroscopic property, is closely related to the atomic thermal amplitudes through the properties of the bonds. Trends of u_1 with bond ionicity have indeed been noted in a previous diffraction study[48] of thermal amplitudes in various III-V compound semiconductors. Recently,[59] ionicities for the CdTe and HgTe bonds in $Hg_{1-y}Cd_yTe$ have been estimated from infrared measurements of TO phonons at very low temperatures ($T=4-6$ K) for various y values. However, no simple relations between the presently measured changes of u_1 with composition for $Hg_{1-y}Cd_yTe$ and the infrared ionicity data of Ref. 59 are apparent.

The strong reduction of u_1 found for Cd and Te in $Zn_xCd_{1-x}Te$ for $x=0.04$, 0.077, and 0.114 with respect to pure CdTe [see Fig. 7(a)] is consistent with the trend obtained from compression measurements, where the bulk modulus of a $Zn_{0.05}Cd_{0.95}Te$ sample was found to be 15% larger than that of pure CdTe.[60] Since the bulk modulus of ZnTe is only 20% higher than that of CdTe,[60] the compression results suggest the existence of a significant upwards bowing of the $B(x)$ curve for the $Zn_xCd_{1-x}Te$ system. This is illustrated in Fig. 9, where bulk modulus values for $Zn_xCd_{1-x}Te$ are plotted as a function of alloy composition x. The solid curve in the figure has been calculated by assuming the empirical bowing equation[61]

$$B_{Zn_xCd_{1-x}Te}(x)=xB_{ZnTe}+(1-x)B_{CdTe}+bx(1-x)\ , \quad (8)$$

where $b>0$ is the bowing parameter. The data points (open squares at $x=0, 0.05, 1$ and for HgTe represent the experimental values available from the literature.[52,60,62] In Eq. (8), the value $b=1.4$ Mbar has been assumed in order to normalize the calculated curve to the experimental data point for $Zn_{0.05}Cd_{0.95}Te$.

For temperatures above the Debye temperature, a power relationship between the thermal amplitude u_1 and B, $u_1\propto B^{\beta}$, where $\beta=-0.5$, may be expected according to the harmonic Debye approximation.[63] Using this power dependence, we can estimate the variations in bulk modulus with x using the present vibrational amplitude data for the crystals studied. However, it was found that in order to obtain a good agreement of B values deduced this way (filled diamond in Fig. 9) with the reported experimental data (open squares), a value of the exponent of $\beta\cong -0.8$, rather than $\beta=-0.5$, has to be assumed. Also noted in Fig. 9 is the fact that the rate of increase in B for

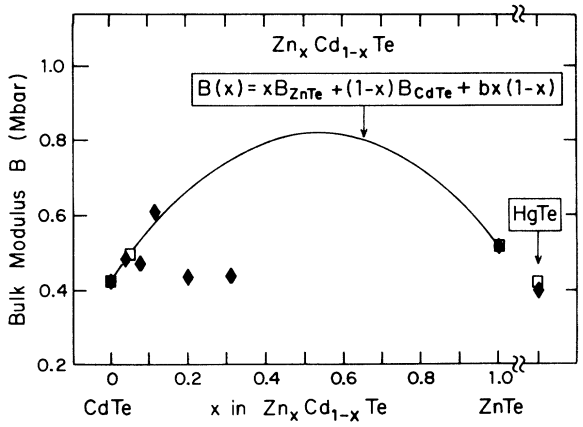

FIG. 9. Bulk modili (B) as a function of composition in $Zn_xCd_{1-x}Te$ and HgTe. □, experimental results from Refs. 52, 60, and 62. ◆, calculated according to the measured changes in u_1 with composition, assuming $u_1\propto B^{-0.8}$ (see text) [normalizing the results to the experimental B value for CdTe ($x=0$)]. Solid curve: calculated $B(x)$ according to Eq. (8).

$0<x<0.114$ as expected from the reduction in u_1 at the same composition range [from Fig. 7(a)] is consistent with that expected from the bowing curve. However, the presently measured thermal amplitudes predict a reduction in B for $x=0.2$ and 0.31, in clear disagreement with the calculated $B(x)$ curve. Unfortunately, no experimental bulk moduli are available for these compositions to resolve this discrepancy.

One of the interesting results obtained from the comparison made in Fig. 9 is the $u_1 \propto B^{-0.8}$ dependence rather than the expected $u_1 \propto B^{-0.5}$.[63] In order to explore this discrepancy, the experimental bulk modulus data for various IV, III-V, and II-VI semiconductors[52] were plotted in Fig. 10 against the experimental thermal amplitude values available from the literature. While a clear correlation between both quantities can be noted in Fig. 10, no single power dependence of u_1 on B is apparent. The slope of the $\log_{10}(u_1)$ vs $\log_{10}(B)$ curve changes from $\beta=-0.9$ for $0.4<B<0.55$ Mbar to $\beta=-0.2$ for $0.55<B<0.9$ Mbar. The covalent semiconductors Si and Ge have lower thermal amplitudes than the binary compounds covering the same range of bulk moduli, and the change in u_1 with B is consistent in this case with $\beta=-0.6$. Note that, in contrast to Fig. 8 where the microhardness for the III-V compounds was found to be shifted to higher values with respect to those of the II-VI materials when plotted as function of u_1, no such "gap" is evident in Fig. 10 between the bulk moduli data for the III-V compounds and those for the II-VI materials. The bulk moduli as expected for the $Zn_xCd_{1-x}Te$ alloys according to Eq. (8) were also included in Fig. 10 for comparison (triangle symbols). It can be seen that these expected values do not follow the trends observed in the figure for the binary compounds. This discrepancy is probably a result of the quadratic bowing assumed in the calculation of B for the $Zn_xCd_{1-x}Te$ alloys [Eq. (8)], which, as can be observed in Fig. 9, may lead to an overestimation of the bulk moduli for $x \gtrsim 0.15$. Indeed, the data point for the $Zn_{0.04}Cd_{0.96}Te$ alloy (closed triangle in Fig. 10) is found to agree well with the general behavior of B as a function of u_1 as shown in the figure.

We have shown above that correlations between the thermal vibrational amplitudes (of the present experiment and of others) and the microhardness (Fig. 8) and bulk modulus (Fig. 10) can be established. By combining the approximate $u_1 \propto H^{-0.26}$ and $u_1 \propto B^{-0.8}$ dependences deduced from Figs. 8–10 for the II-VI materials, a proportionality $H \propto B^3$ is expected to hold for the relationship between the microhardness and bulk modulus. Such a relationship has been studied in the past by several authors for various groups of minerals.[64] In Fig. 11 the microhardnesses for some of the materials considered in Fig. 8 are plotted as functions of the corresponding bulk moduli. It can be seen in the figure that the "gap" between the microhardness values of the IV and III-V semiconductors and those of the II-VI materials observed previously in Fig. 8 is also present when the data are plotted against the corresponding bulk moduli. Furthermore, the dependence deduced from the straight line connecting the data for the II-VI compounds is $H \propto B^{2.9}$, in agreement with the value of 3 expected from Figs. 8–10. The calculated bulk moduli for the $Zn_xCd_{1-x}Te$ alloys based on the present thermal amplitude data and the relationship $u_1 \propto B^{-0.8}$, as deduced from Fig. 9, are also shown in Fig. 11 for comparison.

The atomic displacements measured in the present experiment at room temperature exhibit the same trend with composition as that found from microhardness and bulk modulus measurements. The observed significant stiffening of $Zn_xCd_{1-x}Te$ with low ($x=0.04$–0.11) Zn concentrations as evidenced by the bulk moduli and the thermal amplitude data has not been explained so far. Recently, Chen, Sher, and Berding[65] presented a model for the calculation of the bulk modulus in pseudobinary crystals of the type $A_{1-x}B_xC$. The model, which considers the strain elastic energy contributions to the bulk modulus in the harmonic approximation, fails to explain

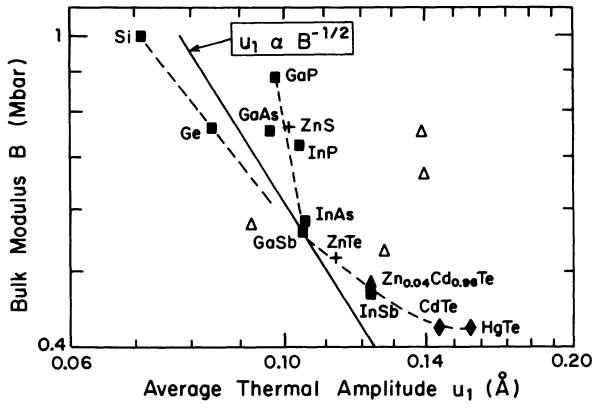

FIG. 10. Experimental bulk moduli B (Refs. 52, 60, and 62) as a function of the average thermal amplitude for various IV, III-V, and II-VI semiconductors. Diamonds and triangles show the present u_1 data. △, data for the $Zn_xCd_{1-x}Te$ alloys, with B calculated from Eq. (8). ▲, $Zn_{0.04}Cd_{0.096}Te$. The dashed lines are guides to the eye, the solid straight line shows the expected $u_1 \propto B^{-0.5}$ dependence normalized to the data point for GaSb.

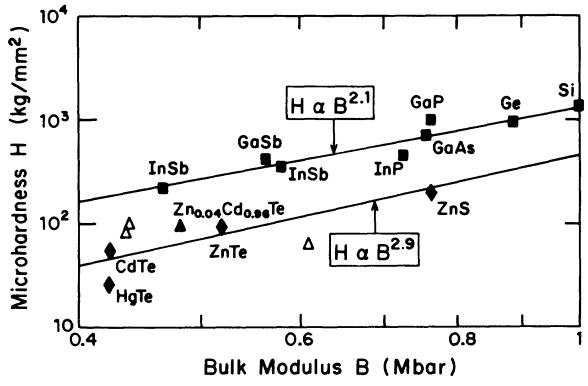

FIG. 11. Microhardness values for the materials considered in Figs. 8–10 plotted as a function of the corresponding bulk moduli. △, data for the $Zn_xCd_{1-x}Te$ alloys with B calculated from the measured u_1, assuming $u_1 \propto B^{-0.8}$. ▲, data for $Zn_{0.04}Cd_{0.96}Te$.

the observed significant increase in bulk modulus for $Zn_{0.05}Cd_{0.95}Te$ relative to CdTe and the upwards bowing of the curve $B(x)$ subsequently expected for $Zn_xCd_{1-x}Te$ (Ref. 60) (see Fig. 9). It is therefore likely that a model which does not neglect the details of chemical bonding and its changes upon composition is needed to explain the effects observed experimentally. Indeed, total energy calculations reported by Wei and Zunger[3] show that details of the bonding structure, including those of the d orbitals, have significant effects on the bulk moduli of II-VI semiconductors and their structural stability.

C. Implication to phonon-dispersion relations

The vibrational amplitudes are determined by a weighted (thermal) average of the various phonon eigenfrequencies of the lattice. The phonon-dispersion relations for the binaries CdTe, ZnTe, and HgTe have been measured by neutron diffraction[16–19] showing that the frequencies of the optic and acoustic branches decrease significantly from ZnTe to CdTe. The dispersion relations of HgTe show optic and acoustic mode frequencies which are just slightly lower than those of CdTe. The acoustic modes at the L and X points in HgTe, however, are significantly lower as a result of the smaller slope of the acoustic branches at low wavelengths. Unfortunately, no neutron diffraction data are yet available for the corresponding pseudobinary alloys. It may be expected, however, that the addition of small amounts of Zn atoms to CdTe to form the $Zn_xCd_{1-x}Te$ alloy will induce local phonon modes at frequencies characteristic to the Zn-Te system, which are higher than the CdTe normal mode frequencies. As a matter of fact, two of these modes have been detected in infrared reflection and absorption studies[66] of $Zn_{0.01}Cd_{0.99}Te$ and $Zn_{0.02}Cd_{0.98}Te$. One local mode (173 cm^{-1}) appears above the LO branches of CdTe. The other, a quasilocal mode (54 cm^{-1}), appears just above the TA branches of CdTe. Furthermore, additional modifications on the CdTe phonon density of states are expected to be induced by the Zn through the strain field produced by the mismatch between the CdTe and ZnTe bond lengths.[67] Since higher frequencies are associated with lower vibrational amplitudes, it is conceivable that the observed reduction in vibrational amplitudes in $Zn_xCd_{1-x}Te$, ($x=0.04,0.077,0.114$) with respect to CdTe is related to the appearance of high-frequency local, quasilocal, or resonant modes in the CdTe vibrational spectrum. It should be noted that for the Zn-rich compositions ($x\rightarrow 1$), for which Cd can be considered as the isovalent impurity added to ZnTe to form the $Zn_xCd_{1-x}Te$ alloy, lower-frequency phonon modes should be induced according to the above argument. The vibrational amplitudes of the Zn-rich alloys should therefore be higher than those of ZnTe. This is indeed consistent with the experimental picture [see Fig. 7(a)]; the values of u_1 found for Zn and Te in $Zn_{0.31}Cd_{0.69}Te$ in the present work are 0.148 and 0.128 Å, while the corresponding u_1 values measured by diffraction methods[27] for ZnTe are 0.126 and 0.099 Å, respectively [see also in Fig. 7(a) the trend of the Mössbauer results in the range $0.35<x<1$]. Therefore a point for which the $u_1(x)$ curve has a minimum and another one where it has a maximum should be expected to occur in the measured compositional dependence of u_1. For $Zn_xCd_{1-x}Te$ and $Hg_{1-y}Cd_yTe$ these are observed at $x\cong 0.11$ and $x\simeq 0.3$ [see Fig. 7(a)], and at $y\cong 0.7$ and $y\cong 0.25$ [see Fig. 7(b)], respectively. A similar behavior has been obtained in diffraction studies[68] of the atomic vibrational amplitudes in $Zn_xHg_{1-x}Te$. The amplitude of Te was found in these studies to decrease significantly from $x=0.13$ to 0.2 (no results for $x=0$ were reported[68]), while increasing slightly when going from ZnTe ($x=1$) to $x=0.75$. A somewhat similar trend was also found in diffraction studies of thermal amplitudes of $In_xGa_{1-x}As$, where the rms displacement of As was found to increase by 15% from $x=0$ to a maximum at $x\cong 0.07$.[69] No results for $x>0.19$ were reported for this system.[69]

D. Temperature dependence of thermal amplitudes

The atomic displacements deduced from measurements at room temperature have been shown to be in general agreement with vibrational amplitudes obtained by others from diffraction methods, and to correlate with data on mechanical properties of the materials studied, such as bulk modulus and microhardness. Additional information on the nature of the atomic displacements measured, including on the possible existence of static contributions, can be obtained by performing temperature-dependent measurements.

Channeling measurements at different temperatures were performed on some of the crystals studied at room temperature as discussed above. Analysis by the Monte Carlo method (method B, Sec. II C) (Ref. 30) of previously reported[50] channeling results obtained at temperatures below room temperature showed that significant underestimation of u_1 may result when neglecting the influence of neighboring crystallographic planes on the $[\bar{1}\,\bar{1}\,\bar{1}]$ axial channeling dips at these temperatures.[70] In the present work, special care was taken to avoid the influence of such planar effects on the measured $[\bar{1}\,\bar{1}\,\bar{1}]$ channeling dips. The channeling results obtained at temperatures below room temperature were analyzed by the simulation method which takes into account such possible effects. Special care was also taken to assure that the composition of the crystals did not change during the lengthy measurements at elevated temperatures. The Hg content of the $Hg_{1-y}Cd_yTe$ samples was monitored in preliminary PIXE experiments by examining the Hg $M_{\alpha\beta}$ peak intensity as a function of temperature. No Hg outdiffusion (e.g., no lowering in the Hg $M_{\alpha\beta}$ peak intensity) was detected below $T=363$ K for $Hg_{1-y}Cd_yTe$ with $y=0$, 0.24, and 0.4; for the $Hg_{0.3}Cd_{0.7}Te$ sample the Hg $M_{\alpha\beta}$ peak intensity remained constant even up to $T=430$ K. The increased stability with respect to Hg loss, observed in $Hg_{0.3}Cd_{0.7}Te$ as compared to the $Hg_{1-y}Cd_yTe$ alloys with other compositions, is most certainly related to the minimum in atomic displacements found at this composition at room temperature [see Fig. 7(b)].

The atomic displacements as a function of temperature deduced for Hg, Cd, and Te in $Hg_{0.76}Cd_{0.24}Te$ are plotted in Fig. 12(a), and compared with the results of the Debye

TABLE II. Debye temperatures in K as determined from the measured atomic displacements for Cd, Te, and Hg for some of the studied crystals, at room (RT) and low (LT) temperatures. The particular temperature of LT in each case is specified in the first column, while RT=296 K. The numbers in parentheses are the expected uncertainties.

	Cd		Te		Hg	
Crystal	RT	LT	RT	LT	RT	LT
CdTe	129	135	135	135		
LT=140 K	(4)	(4)	(4)	(4)		
$Hg_{0.76}Cd_{0.24}Te$	126	131	126	127	86	87
LT=104 K	(4)	(4)	(4)	(4)	(3)	(4)
$Hg_{0.3}Cd_{0.7}Te$	144	135	147	135	103	95
LT=112 K	(6)	(4)	(4)	(2)	(3)	(5)
$Zn_{0.04}Cd_{0.96}Te$	150	182	155	194		
LT=120 K	(6)	(8)	(6)	(10)		
$Zn_{0.114}Cd_{0.886}Te$	184	268	236	304		
LT=126 K	(12)	(17)	(15)	(23)		
$Zn_{0.31}Cd_{0.69}Te$	130	135	143	159		
LT=103 K	(4)	(5)	(4)	(5)		

model (assuming a constant Debye temperature).[71] The Debye model has been shown to describe reasonably well the temperature behavior of the measured thermal amplitudes of Cd and Te in CdTe.[26,50] The agreement between the simple Debye model and the experimental data in Fig. 12(a) for the lower temperatures is acceptable; the deviations of the data points from the lines at the higher temperatures are probably due to the formation of domains with high concentration of Hg vacancies and subsequent lattice disorder, and/or to the increased anharmonic contributions to the lattice vibrations at the corresponding temperatures. Similar data for Cd and Te in CdTe (Ref. 50) and Hg, Cd, and Te $Hg_{0.3}Cd_{0.7}Te$ (not shown) yield also a reasonable agreement with the Debye description. However, the results for the atomic displacements of Cd and Te in $Zn_{0.04}Cd_{0.96}Te$ as a function of temperature [see Fig. 12(b)] show a clear discrepancy between the simple Debye model (lines) and experiment (symbols) at the lower temperatures. Here the experimental data points for both Cd and Te are significantly lower than expected according to the model. The situation is summarized in Table II, where the Debye temperatures for Cd, Te, and Hg as deduced[71] from the experimental atomic displacements at two different crystal temperatures are listed, i.e., at room temperature (RT) and at a lower temperature (LT). For the Debye model to be a reasonable approximation, similar Debye temperatures should be obtained at RT and LT. While this is found to be the case for CdTe, $Hg_{0.76}Cd_{0.24}Te$, $Hg_{0.3}Cd_{0.7}Te$, and $Zn_{0.31}Cd_{0.69}Te$, it is not for $Zn_xCd_{1-x}Te$ with $x=0.04$ and 0.114. For these the Debye temperatures deduced from the atomic displacements as the lower temperature are significantly higher than those deduced from the results at RT. This behavior cannot be explained by postulating contributions to the measured rms displacements of static atomic displacements as these contributions would be reflected in lower Debye temperatures for the lower crystal temperatures, in contrast to the observed trend. It should be pointed out, however, that some care should be taken when considering the u_1 values obtained from channeling measurements at temperatures below RT. At these temperatures the absolute magnitude of atomic displacements deduced are more sensitive to the specific structural model incorporated into the Monte Carlo simulation program.[30] For example, the reduction of the u_1 values with respect to the Debye model found for $Zn_{0.04}Cd_{0.96}Te$ and $Zn_{0.114}Cd_{0.886}Te$ at the lower tem-

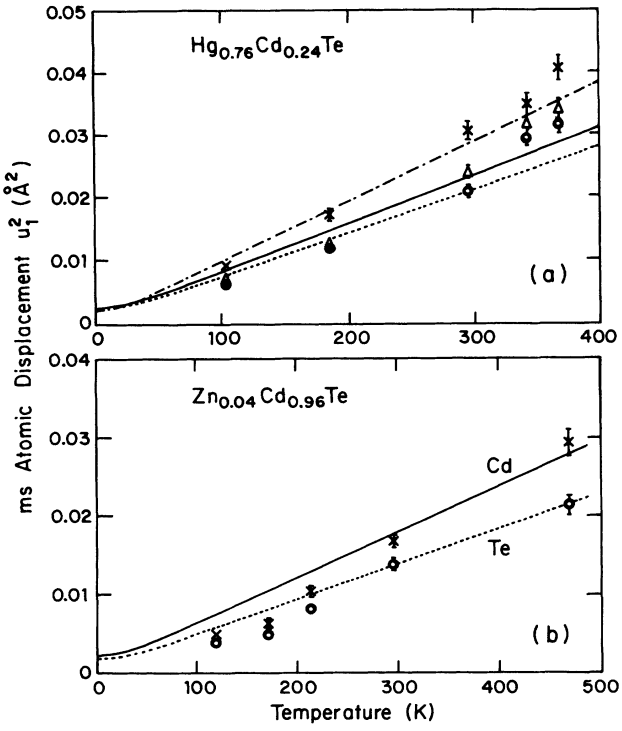

FIG. 12. (a) Mean-square displacements of Hg (×), Cd (△), and Te (○) as a function of temperature in $Hg_{0.76}Cd_{0.24}Te$. (b) Mean-square displacements for Cd (×) and Te (○) in $Zn_{0.04}Cd_{0.96}Te$ as a function of temperature. The lines are values calculated from the Debye model for Hg (dot-dashed line), Cd (solid lines), and Te (dashed lines).

peratures [see Fig. 12(b) and Table II] could result from an overestimation of the static displacements in the structural model assumed. Nevertheless, this does not seem to be the case since the u_1 results obtained for $Zn_{0.31}Cd_{0.69}Te$ (see Table II) do not show the same trend as for $Zn_{0.04}Cd_{0.96}Te$ and $Zn_{0.114}Cd_{0.886}Te$. Furthermore, the channeling results obtained for all the crystals studied were also analyzed by method A, in which static displacements due to bond relaxation are neglected (see Sec. II C). A comparison of the results obtained by both methods showed that absolute magnitudes, but not the obtained trends, may be dependent upon the method used for the analysis of the channeling results.

Interestingly, the crystals which exhibit the enhancement of the Debye temperature at the lower temperatures in Table II, $Zn_{0.04}Cd_{0.96}Te$ and $Zn_{0.114}Cd_{0.886}Te$, are those that show a strong reduction in thermal amplitudes relative to CdTe at room temperature [see Fig. 7(a)]. Since the Debye model is a macroscopic one which does not account for the optical modes or the acoustic modes at the highest frequencies, it is conceivable that deviations from that model will occur whenever the influence of these high-frequency modes in the vibrational spectrum (and hence in the determination of the vibrational amplitudes) becomes significant. The emerging picture is consistent with the argument presented in Sec. III C regarding the strong reduction of the atomic displacements in $Zn_xCd_{1-x}Te$ ($x=0.04,0.077,0.114$), i.e., addition to Zn to CdTe induces modifications to the vibrational spectrum of the lattice, including the local modes at higher frequencies as previously detected in infrared absorption and reflection measurements.[66] These Zn-induced modes probably increase the statistical weight of the higher-frequency phonons in the vibrational spectrum, resulting in both the detected reduction of the thermal vibrational amplitudes with respect to CdTe, and in the deviations from the Debye description evidenced by the temperature-dependent results for $Zn_{0.04}Cd_{0.96}Te$ and $Zn_{0.114}Cd_{0.886}Te$. Further experimental and theoretical work is clearly needed in order to provide a basis for a general understanding of the effects observed here for the crystals studied and their implications to other similar systems.

V. SUMMARY

The thermal vibrational amplitudes of Cd, Te, and Zn in $Zn_xCd_{1-x}Te$ and of Hg, Te, and Cd in $Hg_{1-y}Cd_yTe$ have been deduced from ion channeling measurements combined with RBS and PIXE for various alloy compositions and temperatures. For $Hg_{1-y}Cd_yTe$ the thermal amplitudes were found to change moderately with composition at room temperature, however, a clear minimum exists for $y=0.7$. The above results are found to be consistent with microhardness results available from the literature.[51] For $Zn_xCd_{1-x}Te$ a strong reduction in the thermal amplitudes of all constituent atoms was found upon small additions ($x<0.12$) of ZnTe to CdTe. The above reductions, which has been observed by us previously,[29] is in qualitative agreement with bulk modulus data available from the literature[60] and with u_1 data obtained by diffraction methods.[46] For the $x=0.114$ composition the reduction is particularly strong (i.e., $\sim 40\%$ relative to pure CdTe), and is most significant for the Te atoms. For higher Zn contents ($x=0.2$ and 0.31) the amplitudes of Cd and Te are close to those measured in pure CdTe.

The vibrational amplitudes of Cd in $Zn_xCd_{1-x}Te$, and of Hg in $Hg_{1-y}Cd_yTe$, are found to be larger than those obtained for the other respective atomic constituents in all compositions studied. The amplitudes of Te, on the other hand, are the lowest in both pseudobinary alloys, in agreement with trends observed in various III-V and II-VI binary compounds.[26,28,48]

General correlation between the present thermal amplitudes and microhardness for $Hg_{1-y}Cd_yTe$ has been found, which has been shown to be common to other IV, III-V, and II-VI semiconducting materials. For $Zn_xCd_{1-x}Te$, deviations from the correlation line are attributed to the presence of significant alloy disorder induced by bond relaxation, which is expected to create pinning forces, thus inhibiting dislocation motion and increasing the measured microhardness in these materials.[56,57] The simple correlations obtained between thermal amplitudes and microhardness (Fig. 8) and between bulk moduli and thermal amplitudes (Fig. 10), in conjunction with correlations reported previously between microhardness and bond length and ionicity,[53,58] suggest that microhardness, bulk moduli, and atomic thermal amplitudes may be closely connected through the bonding properties in tetrahedrally bonded semiconductors which are not substantially disordered due to bond relaxation effects.

The dependence of the thermal amplitudes of constituent atoms in $Zn_xCd_{1-x}Te$ and $Hg_{1-y}Cd_yTe$ on composition is still not well understood. It is suggested that the observed reduction in u_1 for $Zn_xCd_{1-x}Te$ with $x=0.04,0.077,0.114$ is related to local and resonant modes induced in the high-frequency regime of the vibrational spectrum of CdTe by the presence of Zn. Even though the observed effect is in qualitative agreement with bulk modulus data,[60] the measured changes in thermal amplitudes with composition cannot be accounted for by the reported changes in bulk modulus by using the simple square-root dependence of the thermal amplitude on the bulk modulus as deduced from the harmonic Debye approximation.[63] A different dependence, which is consistent with the empirical relations between the microhardness and the bulk modulus (Fig. 11) and between the microhardness and the thermal amplitudes [Eq. 7(b), Fig. 8], has been shown to yield better agreement between bulk moduli and thermal amplitudes for the materials studied. Significant deviations from the harmonic Debye model are also observed on the temperature dependence of u_1 in $Zn_{0.04}Cd_{0.96}Te$ and $Zn_{0.114}Cd_{0.886}Te$, which cannot be explained by assuming static contributions to the measured rms displacements. Theories of lattice dynamics reproduce reasonably well the experimental phonon-dispersion relations for semiconducting binary compounds when multiparameter phenomenological models, such as the shell model[16] or the rigid ion model,[17] are used. These models, however, yield calculated thermal

vibrational amplitudes which are in general in disagreement with the corresponding measured values.[72] The behavior of the TO frequencies with composition in the pseudobinary alloys is usually considered within the random-element isodisplacement model by linearly interpolating the phenomenological force constants of the binary constituents.[20,25] However, the force constants between next-nearest neighbors obtained in such calculations[73] are usually found to be of the same order as the force constants between the nearest neighbors. This unphysical result puts in doubt the validity of phenomenological models for the description of vibrational effects, such as those observed in the present work. An *ab initio* theory, which takes into account the changes with composition of the chemical bonding, such as charge transfer between bonds and bond relaxation, and which incorporates the structural and strain effects on the lattice vibrations, should reproduce the observed behavior of the thermal amplitudes with composition and temperature.

ACKNOWLEDGMENTS

The authors would like to thank Dr. E. Muranevich and Dr. R. Triboulet for the supply of the samples. Dr. V. Richter and B. Philosoff are acknowledged for help in the experiments. The authors are indebted to Dr. J. H. Barrett for fruitful discussions and to Professor Alex Zunger for his help on interpretation and suggestions on exploring the scaling relationships between u_1, B, and H. The financial support of the U.S.–Israel Binational Science Foundation (BSF Contract No. 88-00295) is gratefully acknowledged.

---

*Present address: Centre for Electrophotonic Materials and Devices, McMaster University, Hamilton, Ontario, Canada L8S 4L7.

[1]See, for example, R. Dornhaus and G. Nimtz, in *Narrow-Gap Semiconductors,* edited by G. Höhler and E. A. Niekisch (Springer, Berlin, 1983), pp. 119–300.

[2]A. B. Chen, A. Sher, and W. E. Spicer, J. Vac. Sci. Technol. A **1**, 1674 (1983).

[3]S. H. Wei and Alex Zunger, J. Vac. Sci. Technol. A **6**, 2597 (1988); J. Cryst. Growth **86**, 1 (1988).

[4]S. H. Wei and Alex Zunger, Phys. Rev. B **46**, 1662 (1991).

[5]A. Balzarotti, Physica B **146**, 150 (1987).

[6]A. Sher, A. B. Chen, and M. van Schilfgaarde, J. Vac. Sci. Technol. A **4**, 1965 (1986).

[7]C. Y. Fong, W. Weber, and J. C. Phillips, Phys. Rev. B **14**, 5387 (1976).

[8]A. Sher, M. A. Berding, and M. van Schilfgaard, J. Cryst. Growth **86**, 15 (1988).

[9]M. H. Tsai, J. D. Dow, K. E. Newman, and R. V. Kasowski, Phys. Rev. B **41**, 7744 (1990).

[10]N. Motta *et al.,* Solid State Commun. **53**, 509 (1985).

[11]D. B. Zax, S. Vega, N. Yellin, and D. Zamir, Chem. Phys. Lett. **130**, 105 (1987).

[12]K. Besha *et al.,* Phys. Rev. B **36**, 6420 (1987).

[13]See, for example, P. M. Amirtharaj *et al.,* J. Vac. Sci. Technol. A **3**, 226 (1985); A. Compaan, R. C. Bowman, Jr., and D. E. Cooper, Appl. Phys. Lett. **56**, 1055 (1990).

[14]A. Marbeuf, C. Mondoloni, R. Triboulet, and J. Rioux, Solid State Commun. **75**, 275 (1990); R. Nkum, R. Weil, E. Muranevich, L. Benguigui, and G. Kimmel, Mater. Sci. Technol. B **9**, 217 (1991).

[15]R. Weil, R. Nkum, E. Muranevich, and L. Benguigui, Phys. Rev. Lett. **62**, 2744 (1989).

[16]J. M. Rowe *et al.,* Phys. Rev. B **10**, 671 (1974).

[17]P. Plumelle and M. Vandenvyver, Phys. Status Solidi B **73**, 271 (1976).

[18]H. Kepa *et al.,* in *Physics of Narrow Gap Semiconductors,* edited by E. Gornik, H. Heinrich, and L. Palmetshofer, Lecture Notes in Physics Vol. 152 (Springer, Berlin, 1982), p. 275.

[19]M. S. Kushwaha and S. S. Kushwaha, Can. J. Phys. **58**, 351 (1980).

[20]H. Harada and D. I. Narita, J. Phys. Soc. Jpn. **30**, 1628 (1971).

[21]L. K. Vodopyanov and E. A. Vinogradov, Cryst. Lattice Defects **5**, 125 (1974).

[22]D. J. Olego, P. M. Raccah, and J. P. Faurie, Phys. Rev. B **33**, 3819 (1986).

[23]S. Perkovich, L. S. Kim, Z. C. Feng, and P. Becla, Phys. Rev. B **42**, 1455 (1990).

[24]R. Dornhaus and G. Nimtz, in *Solid-State Physics,* edited by G. Höhler and E. A. Niekisch, Springer Tracts in Modern Physics Vol. 78 (Springer, Berlin, 1976), p. 1.

[25]D. N. Talwar and M. Vandenvyver, J. Appl. Phys. **56**, 1601 (1984).

[26]N. N. Sirota and V. D. Yanovich, in *Chemical Bonds in Semiconductors and Thermodynamics,* edited by N. N. Sirota (Consultants Bureau, New York, 1967); A. A. Vaipolin, Fiz. Tverd. Tela (Leningrad) **15**, 1223 (1973) [Sov. Phys. Solid State **15**, 823 (1973)]; R. D. Horning and J. L. Staudenmann, Phys. Rev. B **34**, 3970 (1986).

[27]The u_1 values for ZnTe quoted throughout the present work are averages of the values reported by the following authors: M. J. Cooper, K. D. Rouse, and H. Fuess, Acta Crystallogr. Sec. A **29**, 49 (1973); T. Yamanaka and M. Tokonami, Acta Crytallogr. Sec. B **41**, 298 (1985); J. Bashir, N. M. Butt, and Q. H. Khan, Acta Crystallogr. Sec. A **44**, 638 (1988); J. L. Baudour *et al.,* J. Phys. Chem. Solids **50**, 309 (1989).

[28]E. F. Skelton, P. L. Radoff, P. Volsaitis, and A. Verbalis, Phys. Rev. B **5**, 3008 (1972); C. S. Guenzer and A. Bienenstock, *ibid.* **8**, 4665 (1973).

[29]D. Comedi, R. Kalish, and V. Richter, Phys. Rev. Lett. **61**, 2125 (1988).

[30]D. Comedi, R. Kalish, and J. H. Barrett, Nucl. Instrum. Methods B **63**, 451 (1992).

[31]E. Muranevich, M. Roitberg, and E. Finkman, J. Cryst. Growth **64**, 285 (1983).

[32]J. C. Woolley and B. Ray, J. Phys. Chem. Solids **13**, 151 (1960).

[33]R. Triboulet and Y. Marfaing, J. Cryst. Growth **51**, 89 (1981).

[34]P. F. Fewster, S. Cole, A. F. W. Willoughby, and M. Brown, J. Appl. Phys. **52**, 4568 (1981); P. F. Fewster and P. A. C. Whiffin, *ibid.* **54**, 4668 (1983).

[35]L. C. Feldman, J. W. Mayer, and S. T. Picraux, *Materials Analysis by Ion Channeling* (Academic, New York, 1982).

[36]D. S. Gemmell, Rev. Mod. Phys. **46**, 129 (1974).

[37]D. D. Cohen and M. Harrigan, At. Data Nucl. Data Tables **33**, 255 (1985); M. Shaanan, V. Richter, and R. Kalish, Nucl.

Instrum. Methods B **35**, 319 (1987).
[38]W. M. J. Veigele, At. Data **5**, 51 (1973).
[39]J. H. Barrett, Phys. Rev. B **3**, 1527 (1971).
[40]L. Vegard, Z. Phys. **5**, 17 (1921).
[41]L. Nordheim, Ann. Phys. (Leipzig) **9**, 607 (1931); **9**, 641 (1931).
[42]J. C. Mikkelsen and J. B. Boyce, Phys. Rev. B **39**, 7509 (1983).
[43]Since HgTe and CdTe are nearly lattice matched, $Hg_{1-y}Cd_yTe$ presents small bond relaxation effects [W. F. Pong, R. A. Mayanovich, and B. A. Bunker, Physica B **158**, 617 (1989)]. Therefore deviations from the zinc-blende structure have been neglected in the analysis for $Hg_{1-y}Cd_yTe$.
[44]A. Qteish, N. Motta, and A. Balzarotti, Phys. Rev. B **39**, 5987 (1989); see also Ref. 3.
[45]M. L. Balciuniene, A. K. Dragunas, and K. V. Makariunas, Litov. Fiz. Sb. **19**, 713 (1979) [Sov. Phys.-Collect. **19**, 68 (1979)].
[46]R. Nkum, Ph.D. thesis, Technion-Israel Institute of Technology, 1988.
[47]Y. Madhavan, K. Ponnammal, K. Ramachandran, and T. M. Haridasan, Phys. Status Solidi B **162**, 119 (1990).
[48]O. H. Nielsen *et al.*, Z. Phys. B **52**, 99 (1983).
[49]R. D. Huiszoon and P. P. M. Groenewegen, Acta Crystallogr. Sec. A **28**, 170 (1972).
[50]D. Comedi and R. Kalish, J. Cryst. Growth **101**, 1022 (1990).
[51]S. Cole, M. Brown, and A. F. W. Willoughby, J. Mater. Sci. **17**, 2061 (1982); M. Schenk and A. Fissel, J. Cryst. Growth **86**, 502 (1988).
[52]R. G. Goble and S. D. Scott, Can. Mineral. **23**, 273 (1985).
[53]A. Sher, A. B. Chen, and W. E. Spicer, Appl. Phys. Lett. **46**, 54 (1985).
[54]M. J. Cooper, K. D. Rouse, and H. Feuss, Acta. Crystallogr. Sec. A **29**, 49 (1973).
[55]J. C. Phillips, *Bonds and Bands in Semiconductors* (Academic, London, 1973).
[56]K. Guergouri, R. Triboulet, A. Tromson-Carli, and Y. Marfaing, J. Cryst. Growth **86**, 61 (1988).
[57]H. Ehrenreich and J. P. Hirth, Appl. Phys. Lett. **46**, 668 (1985).
[58]N. A. Goryunova, A. S. Borshchevskii, and D. N. Tretiakov, in *Semiconductors and Semimetals,* edited by R. K. Willardson and A. C. Beer (Academic, London, 1968), Vol. 4, Chap. 1.
[59]S. Perkovich, L. S. Kim, and P. Becla, Solid State Commun. **77**, 471 (1991).
[60]S. B. Qadri, E. F. Skelton, A. W. Webb, and J. Kennedy, Appl. Phys. Lett. **46**, 257 (1985); J. Vac. Sci. Technol. A **4**, 1971 (1986).
[61]See, for example, N. A. Goryunova, A. S. Borshchevskii, and D. N. Tretiakov, in *Semiconductors and Semimetals* (Ref. 58), and Refs. 22 and 43 therein.
[62]S. B. Qadri, E. F. Skelton, A. W. Webb, and J. Dinan, J. Vac. Sci. Technol. A **4**, 1974 (1986).
[63]V. M. Glazov, Zh. Fiz. Khim. **45**, 2719 (1978) [Russ. J. Phys. Chem. **45**, 1543 (1971)].
[64]See Ref. 52, and references therein.
[65]A. B. Chen, A. Sher, and M. A. Berding, Phys. Rev. B **37**, 6285 (1988).
[66]W. Lu *et al.*, Solid State Commun. **64**, 1167 (1987); Phys. Status Solidi B **147**, 767 (1988).
[67]D. N. Talwar, Philos. Mag. B **56**, 593 (1987).
[68]J. L. Baudour *et al.*, J. Phys. Chem. Solids **50**, 309 (1989).
[69]U. Pietsch, Phys. Status Solidi B **107**, 185 (1981).
[70]This was found to be the case for the u_1 data reported previously for $Hg_{0.76}Cd_{0.24}Te$ [see Fig. 4(b) of Ref. 50].
[71]A. A. Maradudin, E. W. Montrol, G. H. Weiss, and I. P. Ipatova, *Theory of Lattice Dynamics in the Harmonic Approximation,* 2nd ed. (Academic, New York, 1971), Suppl. 3.
[72]See, for example, D. N. Talwar and B. K. Agrawal, J. Phys. C **7**, 2981 (1974); J. F. Vetelino, S. P. Gaur, and S. S. Mitra, Phys. Rev. B **5**, 2360 (1972); J. S. Reid, Acta. Crystallogr. Sec. A **39**, 1 (1983).
[73]D. N. Talwar and T. D. Fang, Phys. Rev. B **41**, 3746 (1990).